

Structural and Mechanical Properties of Polyelectrolyte Multilayer Films Studied by AFM

Ozzy Mermut, Julie Lefebvre, Derek G. Gray, and Christopher J. Barrett*

Department of Chemistry, McGill University, 801 Sherbrooke Street West, Montreal H3A 2K6, Canada

Received July 9, 2003; Revised Manuscript Received September 18, 2003

ABSTRACT: Mechanical properties of polyelectrolyte multilayer thin films were studied by nanoindentation experiments using an atomic force microscope. We obtained force–distance measurements for a model polycation/polyanion multilayer system, poly(allylamine hydrochloride) (PAH), and an azobenzene-containing polyelectrolyte (P-Azo) prepared at varying charge densities. The relative Young's modulus of the films was determined as a function of the ionization fraction of the multilayer films, prepared to have identical thickness. Multilayer films assembled with polyelectrolytes of high charge density exhibited an elastic modulus that was significantly larger (nearly 2 orders of magnitude) than those prepared with low charge density. An estimate of the relative loop length between "ionic cross-links" in the multilayer films is then ascertained by analogy to previously studied covalently cross-linked polymer networks. The modulus values in our films ranged from 10^{-2} to 10^{-4} kPa, and this implies loop lengths of 1–50 segments. Atomic force microscopy force–distance measurements were also used to compare the relative adhesion values between polycation and polyanion layers in films constructed with varying charge densities. This was done by coating an AFM tip with multilayers and indenting into a surface containing the same multilayer film but capped with the oppositely charged surface polyelectrolyte layer. Adhesion values were typically between 0.5 and 6.7 nN and were found to depend on the ionic cross-link density of the PAH/P-Azo film, in which the highly ionically cross-linked samples exhibited the largest adhesion.

Introduction

The sequential assembly of oppositely charged polyelectrolytes in an alternating layer-by-layer fashion has recently become a useful tool for the controlled fabrication of organic thin films and modification of surfaces in aqueous media.^{1,2} The promise of these multicomposite organic films as viable materials in various applications such as separation membranes and drug delivery capsules relies on the ability to direct the internal architecture of the multilayers on a molecular level.^{3,4} For example, controlling structural properties such as the density or porosity of a multilayer film is critical for their use as antireflection optical coatings,⁵ biocompatible macromolecule encapsulates,^{6,7} and gas separation membranes,⁸ since the architecture governs the refractive index, molecular diffusion rates, and gas permeability, respectively, in the film. Furthermore, the use of weak polyelectrolytes allows flexibility in the film architecture, which can be defined during either the multilayer preparation through pH adjustments of the polymer ionization fraction or post-self-assembly via pH-mediated porosity transitions.⁹

Early on in the study of polyelectrolyte multilayer assemblies it was shown that, in cases where the polyions of constant charge density are used, the ionic strength of the adsorption solutions is a significant factor in determining both the conformation of the adsorbing polyelectrolytes^{10–12} and the thickness of the adsorbed layers.^{13,14} More recently, it has been demonstrated that the employment of weak polyelectrolytes (i.e., those containing pH-dependent charge density in aqueous solution) is highly advantageous due to the ability to control the layer thickness by tuning the ionization fraction of the polyions about their pK .^{15–17} The diverse range of solution-dependent conformational

properties that polyelectrolytes can adopt when forming multilayer assemblies have prompted several investigations aimed at examining the internal architecture of the films. Previously, X-ray and neutron reflectometry experiments have been used for small-scale structural elucidation of the films (i.e., on the order of 10 nm).^{2,18} For instance, neutron experiments have been used to probe concentration gradients along the layer normal, thus revealing information about the extent of stratification of the layers, the interfacial roughness, and the degree of interpenetration between subsequent layers.^{19,20} However, these high-energy techniques are inefficient, requiring deuteration of the sample, and are unable to measure contact-point density in multilayer films. Optical methods such as second harmonic generation (SHG) have also been useful for probing interfacial properties of anisotropically oriented polyelectrolyte layers,^{21,22} while optical waveguide light mode spectroscopy (OWLS) and scanning angle reflectometry (SAR) have also been employed to obtain structural information on multilayers.²³ While many of these techniques have been successful at characterizing the interfaces and layer architecture in the films, there is still a lack of understanding concerning some of the basic structural properties of the polymer chains forming the ionic links between the layers, i.e., the loop length between "ionic cross-links". Obtaining such information as a function of assembly conditions has proved difficult, and this task is further complicated by the presence of significant interpenetration observed between adjacent layers,² as revealed by reflectivity studies¹¹ and Foerster energy transfer experiments.²⁴

Previous atomic force microscopy (AFM) studies of polyelectrolyte multilayers have focused primarily on visual characterization of the thin films in response to various assembly parameters such as the number of layers built,²⁵ solution salt,²⁶ pH conditions,²⁷ intermit-

* Corresponding author: e-mail chris.barrett@mcgill.ca.

tent drying between adsorption cycles,²⁸ and the effect of postassembly exposure to electrolyte solution.^{5,9} Extensive AFM investigations into various polyelectrolyte multilayer systems in the image mode have revealed much information regarding surface properties such as aggregation,²⁹ homo/heterogeneity,³⁰ roughness,³¹ coverage,³⁰ and porosity.⁹ However, relatively few investigations have been conducted on the mechanical properties of layered polyelectrolyte films, in particular by AFM force–distance measurements. A few notable exceptions to this have involved using an AFM in force mode to measure dynamic interactions and friction in adsorbed single polyelectrolyte layers.^{32,33a,b} Gravimetric techniques such as quartz crystal microbalance (QCM) have also been used for mechanical characterization of the film–solution interface in polyelectrolyte multilayers via acoustic impedance measurements of a multilayered resonator. In a recent report, the viscoelastic behavior of the outermost diffuse layers in polyelectrolyte multilayer films was determined using QCM measurements, and the shear modulus of the film's surface was investigated as a function of ionic strength, intrinsic polyion flexibility, and variable terminating polymer layer.³⁴ In addition, the surface force apparatus (SFA) has been a suitable tool for in-depth examinations of the interaction forces and shear properties of adsorbed polyelectrolyte layers³⁵ and multilayers.³⁶

In this study, we obtained elasticity measurements from the indentation curves of an AFM tip into a series of PAH/P-Azo multilayer films, prepared at various pH conditions, to probe the mechanical nature of the polymer layer structures resulting from assembling weakly charged polyelectrolytes at various charge densities. The elastic modulus is then determined from the force–distance data by fitting the deformation in the contact region to Hertzian mechanics. A structure–mechanical property relation in the polymer films is inferred by relating the “ionic cross-link” density (frequency of connection points between oppositely charged polyions in the multilayer) to the resulting elastic response. Consequently, we propose that mechanical force–distance measurements made using an AFM may be successfully and systematically applied in order to compare relative polymer loop length between “ionic cross-links” formed during the assembly of weak polyions into multilayer films, a measurement difficult to obtain by any other technique.

Experimental Section

Materials. The weakly charged polycations and polyanions assembled into multilayer films were PAH (Polysciences, M_w 60K), and P-Azo (Aldrich, M_w 90K), respectively. The chemical structures of these polyelectrolytes are shown in Figure 1. Aqueous solutions containing 10^{-2} M per polyion repeat unit were prepared using 18 M Ω cm resistivity Millipore Milli-Q water. The charge density of the polyelectrolytes was adjusted by altering the pH of the assembly solutions from a value of 5.0 to 10.5 using NaOH or HCl. The pH of the polymer solutions was periodically monitored and did not deviate more than ± 0.2 pH units over the course of film fabrication.

Multilayer Film Preparation. The substrates, Si (Wafertec) and glass slides (Fisherbrand), were cleaned by immersion in a bath of 25% H₂SO₄ and 75% H₂CrO₄ for 24 h. To rid the substrates of chromium and other ions, the surfaces were rinsed with a concentrated solution of HCl followed by thorough rinsing with Milli-Q water. The average contact angle of the surfaces was measured to be $<10^\circ$ (Optrel GBR Multiskop), ensuring that the substrates were hydrophilic

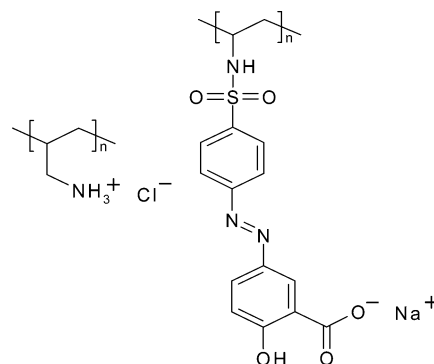


Figure 1. Repeat unit structures of the polycation, PAH (left), and the polyanion, P-Azo (right), used.

prior to deposition of the initial polycation layer. The film assembly procedure involved the alternating and repeated immersion of substrates in polycation solution, followed by the polyanion solution. Between each polyelectrolyte deposition, films were rinsed in several baths of Milli-Q water. It is known from previous time-dependent studies of various weak polyelectrolyte systems into multilayer assemblies that saturated adsorption in these systems ($>80\%$) is readily achieved in <1 min.³⁷ Thus, multilayer films were constructed using a dipping time of 2 min for both polyelectrolyte solutions. Using an automatic slide stainer (Shandon), multilayer films were prepared with polyions having varying charge densities using solutions adjusted to pH values of 5.0, 7.0, 9.0, and 10.5 (matched for both polycation and polyanion) and depositing 346, 560, 116, and 76 layers, respectively, to make films of identical thickness (1100 ± 60 nm) on Si. A Gaertner ellipsometer at 633 nm (calculating both refractive index and layer thickness) was used to measure the film thickness on Si. We also confirmed that films assembled on glass slides at varying pH values were similar in optical thickness by observing the $\pi \rightarrow \pi^*$ absorbance maximum of P-Azo at $\lambda_{\max} = 365$ nm using a UV–vis spectrophotometer (Varian Cary 300-Bio; scan rate 100 nm min⁻¹).

For adhesion measurements, silicon nitride tips (Veeco, DNP probes) were modified with 75 layers of PAH/P-Azo, prepared by dipping in polycation/polyanion solutions matched at either pH = 5.0 or pH = 9.5. In all cases, the capping layer of the multilayered probe was PAH. The multilayered AFM probes and reference uncoated tips were imaged with a scanning electron microscope (SEM, JEOL 840A) at 10 000 \times magnification.

Elasticity Measurements Using an AFM. Force measurements of the multilayer films were performed using an AFM in force calibration mode (Nanoscope Version 3A, Digital Instruments). The multilayer surface and the tip were brought together in a fluid cell at room temperature. We used silicon nitride probes ($r = 20$ – 60 nm) with a manufacturer specified force constant, k , of 0.12 N/m. All elasticity measurements of the films were performed with the same AFM tip; thus, no calibration for the absolute spring constant of the tip was performed. The AFM detector sensitivity was calibrated by obtaining a force curve on a bare substrate and determining the slope of the linear portion of the data after contact. Obtaining force curves of the multilayer film involved bringing the tip in close contact with the surface in aqueous media and obtaining force measurements after allowing the system to equilibrate for 10 min or until reproducible curves were observed. The rate of the indentation cycle was kept constant at 0.2 Hz. For elasticity measurements, four replicate measurements of the deflection as a function of the piezo z -position were acquired with the unmodified AFM tip indented at random coordinates on the film surface.

Data Analysis of Force Curves. Similar to previously described methods, we analyzed our AFM data by first characterizing the three main regions in the deflection curve, which depict the interaction of the tip with the substrate (on both the approach and the retraction).^{38,39} In the noncontact

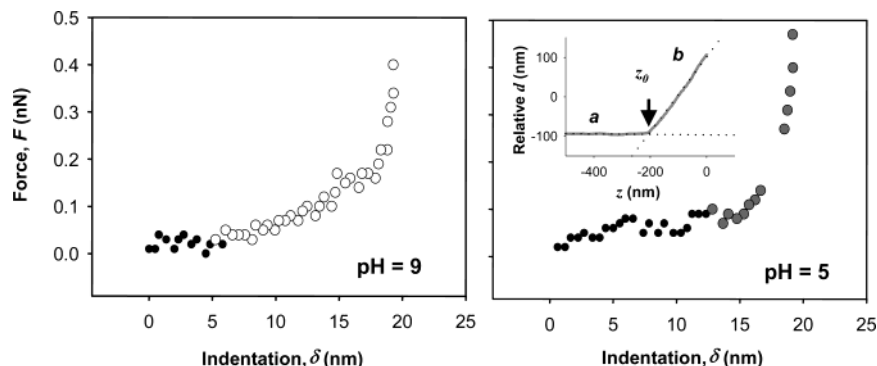


Figure 2. Force as a function of indentation after the tip contacts a multilayer film prepared with low charge density (pH = 9.0) and strongly charged (pH = 5.0) PAH. Empty and gray shaded circles represent the region where the indentation obeys Hertzian deformation mechanics for the respective systems. The inset illustrates a typical deflection vs z -position raw approach curve.

region, the tip and surface do not interact with one another, except in the case of long-range forces, and thus no change in the cantilever deflection, d , is detected with respect to z -position of the piezo, z . After contacting the surface, deflection of the probe begins to increase, and this characterizes the nonlinear contact region. Provided that the film is sufficiently soft, the tip will indent the sample to a distance, δ , resulting in a smaller deflection with $d = z - \delta$. At some point in the indentation, the cantilever deflection becomes linear with respect to z , upon which $d = z$, indicating that “infinite stiffness” in the sample has been reached. While a more rigorous approach using SFA can yield an absolute value for the true separation between the tip and the sample, the contact or zero point, z_0 , in AFM is ascertained graphically as the initial point where the noncontact region of the curve begins to deviate from linearity. In practice, the z_0 is obtained as the intersection coordinate between the extrapolated linear pre-contact region (part a in the deflection curve, inset of Figure 2) with the extrapolated “infinitely stiff” portion of the contact region (part b).⁴⁰ All force measurements were obtained in 10 mM NaCl (i.e., at pH = 5.0, below the pK_a of the Si_3N_4 tip of 6.0).⁴⁰ Under these conditions, there was more efficient screening of adhesion (observed in the retraction curve when using Milli-Q water) and reduced tip-sample interactions resulting in tip instability, (i.e., near z_0 in the approach curve). Note that for ease of comparing the force data the curves were rotated to remove elements of long-range repulsive forces, a procedure which results in flattening the force curves.

To convert the raw deflection vs z -position data into a plot of force as a function of indentation, we use Hooke's law in which the loading force, F , is related to the deflection through the cantilever force constant.³⁸

$$F = kd = k(z - \delta) \quad (1)$$

A final force vs separation plot is thus obtained by (a) calibrating the sensitivity, (b) shifting the deflection curve to the appropriate (0,0) contact point, (c) converting the z movement of the piezo to an indentation, and (d) using Hooke's law to convert deflection into force.

We used Hertzian mechanics to describe the elastic deformation of the multilayer film (assumed to be a planar surface) with a spherical tip (fit to this geometry based on indentation depths into the multilayer which were less than the tip radius). Young's modulus, E , can then be calculated from the following equation:³⁹

$$F = \frac{4E\sqrt{r}}{3(1 - \sigma^2)} \delta^{3/2} \quad (2a)$$

We assume that the multilayer polymer film behaves as an elastic rubber and thus imposes a Poisson ratio of $\sigma = 0.5$. The average specified tip radius was $r \sim 40$ nm. In a linear plot of $\log F$ as a function of $\log \delta$, the elastic modulus is then extracted from the intercept value as suggested by eq 2b. Note that while we observed little hysteresis between the approach

Table 1. Structural Properties of PAH/P-Azo Multilayer Films as a Function of Preparation pH

prepn pH	h/m_L (Å)	E (kPa)	ρ/M_x (mol/m ³)	% rel ρ/M_x	rel loop length
5	3.0	6500 ± 900	870	100	1
7	2.0	1800 ± 1000	240	28	4
9	9.2	120 ± 60	17	2	50
10.5	18	170 ± 40	23	3	33

and retract cycle of the nanoindentation, we analyzed the approach curves due to interference of adhesion forces exhibited during the retraction of the tip. To determine the elastic modulus of the films, the force curves in the contact region were fitted to eq 2b by fixing the slope to $3/2$ (with all experimental $r^2 > 0.92$) and solved for the intercept value, b .

$$\log F = \frac{3}{2} \log \delta + \log \left(\frac{4E\sqrt{r}}{3(1 - \sigma^2)} \right) \quad (2b)$$

For the adhesion experiments, measurements of the pull-off force between a multilayered tip and multilayer films on glass slides were conducted in both Milli-Q water and 10 mM NaCl. The average adhesion values were compared for three assembly pH combinations for both the tip and the substrate (a minimum of 20 random measurements per sample over a $10 \times 10 \mu\text{m}$ area).

Results and Discussion

Elastic Modulus of Multilayer Films. It has previously been established that the thickness of a multilayer film assembled from weakly charged PAH and P-Azo is dependent on the ionization fraction of the polyelectrolytes during assembly, in particular, that of PAH.³⁷ For example, when PAH/P-Azo films are prepared using a solution pH above that of the pK_a of PAH, i.e., pH ~ 8.7 ,⁴¹ the per layer optical and ellipsometric thickness of the film increases significantly as compared to the film constructed with PAH when it is strongly charged at pH = 5.0 and pH = 7.0, as indicated in Table 1. Using an atomic force microscope, nanoindentations of PAH/P-Azo were performed on identically thick films to determine the relative Young's modulus as a function of the polyelectrolyte charge density during assembly. For comparison, Figure 2 shows representative force vs indentation curves obtained for films prepared above and below the pK_a of PAH. Indentation of the films was typically < 50 nm, thus restricting the fit of Hertzian deformation mechanics to a spherical tip geometry.³⁹ Analyzing the contact region of the approach curves and applying eq 2b, we determined the elastic modulus of the films via the intercept value of the plot of $\log F$ vs

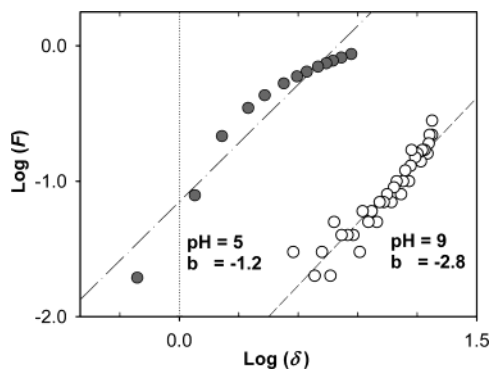


Figure 3. Plots of $\log F$ vs $\log \delta$ for the multilayer films fit to Hertzian mechanics. From eq 2b, the elastic modulus is determined by the intercept value, b , where $\log \delta = 0$.

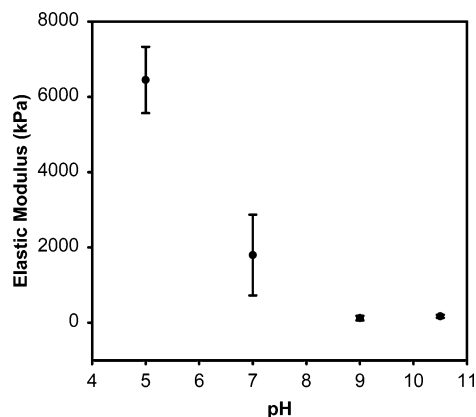


Figure 4. Elastic modulus of PAH/P-Azo films as a function of the assembly pH.

$\log \delta$. The elasticity for films made at pH = 9.0 and pH = 5.0 was found to be 6.7×10^{-3} and 1.2×10^{-4} nN/nm², respectively, as displayed in Figure 3. Similarly, we obtained force vs indentation data for films prepared at pH = 7.0 and pH = 10.5. Since the indentation depth (≤ 50 nm) is much smaller than the film thickness (~ 1100 nm), we assume negligible substrate effects in the determined elasticity. Figure 4 shows the average elastic modulus of the four films, determined by averaging four unique sets of measurements at each pH value. It was observed that both the films prepared pH = 5.0 and pH = 7.0 (i.e., employing strongly charged PAH) exhibit a Young's modulus, which is on the order of 50 times greater than that of the multilayers constructed at pH = 9.0 and pH = 10.5 (i.e., assembling with weakly charged PAH).

The range of elastic modulus values for the entire series of PAH/P-Azo multilayer films analyzed was determined to be on the order of 10^2 to nearly 10^4 kPa, with modulus increasing as the assembly pH was decreased. The magnitude of our results agrees with a recent QCM study of high molecular weight PSS/PDADMA films containing ≤ 10 layers where the "softness parameter" was found to be between 10^2 and 10^3 kPa for the strongly charged system and shown to increase with the number of layers deposited.³⁴ In fact, the observed range in the elasticity for PAH/P-Azo multilayers of low and high ionic cross-link density is comparable to that of adsorbed mussel adhesive protein layers before and after covalent cross-linking, respectively.⁴² It appears that reducing the charge density of PAH results in multilayer films having elastic behavior, which resemble that of hydrogel-type layers.

The buildup of polyelectrolyte multilayers is known to result from the formation of a large number of weak ionic interactions (i.e., on the order of kT) established between cationic and anionic groups of the polyelectrolytes.⁴³ For polyelectrolytes assembled at high and low charge density, the number of ionized groups and hence the percent of "ionically cross-linkable" groups between layers are different in the two cases. This implies that the relative loop length between ionic cross-links in multilayer films may be inferred from the differences in the elastic behavior of the films as a consequence of varying the polyelectrolyte charge density. In essence, we can use AFM force-indentation data to obtain information on the internal architecture of the film, specifically the density of the ionic cross-links connecting the layers via the positive and negative repeat units of the two polyelectrolytes. In the ideal and simplest case of vulcanized rubber (i.e., ignoring effects of "loose ends" of molecules), the relation between the degree of covalent cross-linking and the resulting network elasticity has previously been described by the following equation:⁴⁴

$$G = \frac{1}{3}E = \frac{\rho RT}{M_x} \quad (3)$$

where G is the modulus of rigidity, ρ/M_x is the density of cross-links, and k , R , and T have their usual Boltzmann definitions. Here, we extend this equation to correlate the elastic behavior of the multilayer films to the average density of "ionic cross-links". Since G and E are directly proportional to the density of cross-links, a 50-fold increase in the observed modulus of PAH/P-Azo, resulting from decreasing the solution pH from a value of 9.0 to 5.0, corresponds to an increase in the ionic cross-link density by 50 times. Given that at solution pH = 5.0 PAH is significantly below its pK_a value, we assume that PAH is 100% charged at this pH and therefore is 100% cross-linked (every segment is paired). While QCM studies have shown evidence for the formation of a small degree of loops in even strongly charged polyelectrolyte layers adsorbed onto gold,⁴⁵ our assumption is valid for determining a relative comparison of a loop length with respect to charge density. Therefore, by normalizing the ionic cross-link density relative to the 100% cross-linked case, we have an estimate of the average relative loop length between the ionic cross-links for the various assembly pH conditions examined (Table 1). From the inference of the corresponding average loop length, we find that in the case of employing weakly charged polyelectrolyte polymer layers of 30–50 times the loop size of the strongly charged species are produced. The results in Table 1 also indicate that AFM nanoindentation experiments can clearly distinguish between high and low cross-link density samples of the multilayers (i.e., attributed to use of strongly vs weakly charged polyelectrolytes respectively). However, while pH = 10.5 films are nearly twice the thickness per layer, h/n_L , of pH = 9.0 multilayers, AFM elasticity measurement are unable to clearly differentiate between varying degrees of ionic cross-links formed from a range of weakly charged polyelectrolytes (i.e., between pH = 9.0 and pH = 10.5).

Multilayer Adhesion and Charge Density. We also used AFM to measure the relative adhesion forces between even and odd layers in PAH/P-Azo films as a function of the ionization fraction of the polyelectrolytes.

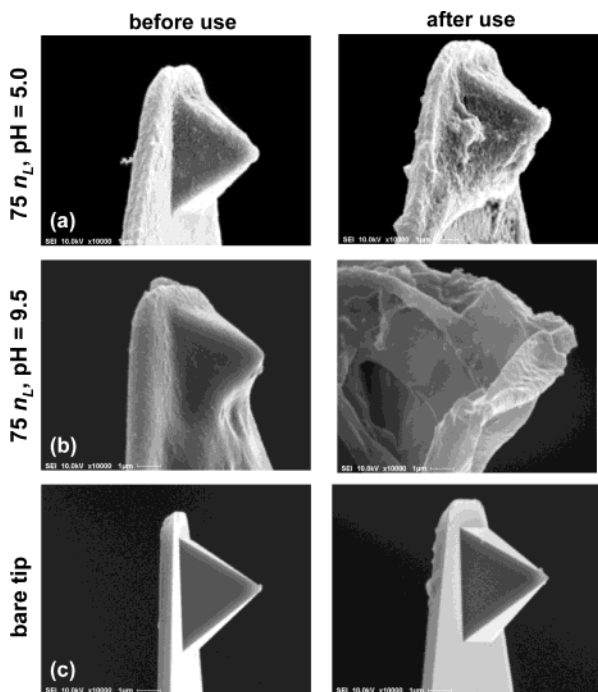


Figure 5. SEM micrographs (10000 \times magnification) of Si_3N_4 tips modified with 75 layers, n_L , of PAH/P-Azo using (a) assembly bath pH = 5.0 and (b) assembly bath pH = 9.5. Sample c is a representative bare Si_3N_4 reference tip. The left and right columns show images of the tips prior to and after adhesion measurements, respectively.

To compare the strength of interactions between identically thick multilayer films prepared at pH = 5.0 versus that at pH = 9.5, we obtained force curves between multilayers assembled on glass slides and an AFM tip also modified with 75 PAH/P-Azo multilayers. While quantitative comparisons between various AFM probes are possible when tips are calibrated, relative adhesion measurements with the same AFM probe are preferable, since effects due to tip imperfections and variations in geometry are identically propagated with all samples examined. However, in the case of a multilayered AFM probe, even use of the same tip may introduce complications in comparing multiple adhesion measurements. Specifically, one cannot be sure that a multilayer-modified AFM probe remains constant between consecutive in situ nanoindentations into a surface also containing polyelectrolyte multilayers. To determine the severity of this problem, the multilayered AFM tips were imaged by SEM to qualitatively characterize and compare the tips before and after adhesion measurements were acquired. As displayed in Figure 5, polymer layers are indeed adsorbed onto the tip, and the structure of the adsorbed layers appears to depend on the assembly pH. In agreement with our previous studies of PAH/P-Azo on flat Si wafers, the SEM micrographs show that much thicker polymer layers are obtained in the case of multilayers prepared at pH = 9.5 compared to those at pH = 5.0. The SEM micrographs also suggest that while bare tips are not significantly altered by the adhesion measurement procedure, noticeable differences in the nature of the polymer-coated tips are observed before and after the tips are engaged in force measurements. The images presented are typical of those obtained for replicate multilayers assembled onto various other Si_3N_4 tips. We speculate that contact of the positively charged PAH surface layer

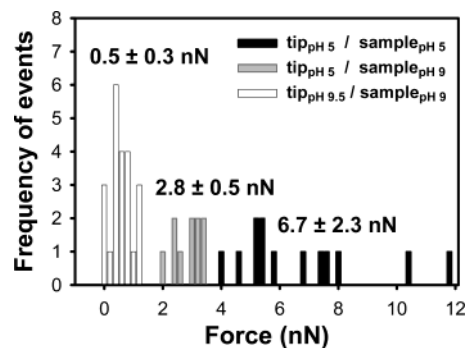


Figure 6. Relative adhesion between PAH/P-Azo multilayers on a tip and on a multilayered surface.

on the tip with the negatively charged P-Azo surface layer on glass, in an aqueous environment, results in the exchange of multilayers.

To survey the relative adhesive forces in layers of PAH/P-Azo films, we constructed adhesion histograms for the multilayered tip and glass surface in the case of both weakly and strongly charged PAH and in the various electrolytic environments. A significant difference was observed in the adhesion of a multilayered tip_{pH 5} and surface_{pH 5} when measured in 10 mM NaCl (average adhesion force of 6.7 nN, displayed in Figure 6) as compared to Milli-Q water (average adhesion force of 1.4 nN, results not shown). These results suggest that the interaction forces, measured between oppositely charged polymer layers of the indenting tip and the surface, are highly dependent on the electrolyte environment. The study also shows that a markedly large variance in the distribution of adhesion forces is obtained in the former case, as indicated in Figure 6. Although different tips were used in the assembly of multilayers at pH = 5.0 and pH = 9.5, the adhesion between various tips prepared at pH = 9.5, and substrates multilayered at pH = 9.5, consistently resulted in lower adhesion values than any combination of tip or surface employing polyelectrolytes assembled at pH = 5.0.

One might expect that the adhesion forces between the PAH capped tip multilayers and the P-Azo capped substrate multilayers depend on the acid–base properties of cationic and anionic functional groups. For example, the relative adhesion strength might be analogous to monolayer systems, which have previously demonstrated pK -dependent interaction between a carboxyl-functionalized AFM tip and substrate.⁴⁶ In such a case, the adhesion would be dominated by the free functional units, i.e., those not involved in forming ionic cross-links. This implies that multilayer films prepared with weakly charged polyelectrolytes would exhibit larger adhesion than strongly charged systems due to a larger density of free functional groups, which are fully ionized in the measurement solution of pH = 5.2. However, we observed the opposite trend. The weakly charged polyelectrolytes exhibited the smallest adhesion upon bringing the tip–substrate multilayers in contact. It is speculated that the reduced adhesion values observed in this case may be an effect of the different film architecture attributed to the reduced ionization fraction of PAH during multilayer assembly on the AFM probe. Elasticity measurements have demonstrated that PAH/P-Azo multilayers on an AFM tip constructed at pH = 9.5 exhibit a reduced cross-link density in precursor layers compared to samples prepared at pH = 5.0.

Since the adhesion is much stronger in the case of pH = 5.0, we believe that multilayers between the tip and substrate are exchanging in situ during the adhesion measurement. Consequently, the force required to break the interactions between the layers is much greater in the case of pH = 5.0, assuming that the dominant interaction force in the multilayers is ionic. This result is consistent with the SEM data, which suggests the occurrence of mass transfer between multilayers on the tip and the substrate during subsequent force measurements (Figure 5).

Conclusions

The elasticity of polyelectrolyte multilayer films as a function of polymer charge density during assembly can be successfully probed with force–distance measurements using an AFM. The modulus of elasticity in turn reveals the average “loop length” between the “ionic cross-links” at the interface between the layers, thus allowing a straightforward method for comparing the internal architecture of the multilayers constructed at varying pH values. In the case of multilayers made from weakly charged PAH and P-Azo (a condition producing thick layers), we found that the relative loop length can be up to 50-fold greater than an identical system prepared using strongly charged polyelectrolytes (resulting in much thinner layers). We also demonstrate that in situ measurements of adhesion forces between multilayered AFM probes and planar multilayered surfaces provide an estimate of the relative strength of layer-to-layer interaction as a function of the bulk ionic cross-link density of the film. While we suspect that a significant degree of mass transfer of layers occurs between the multilayered tip and surface during these AFM adhesion measurements, we consistently observed much lower adhesion forces in all cases of multilayers prepared from weakly charged polyelectrolytes. This suggests that the employment of fully ionized polyelectrolytes result in multilayers, which as a bulk appear to be more strongly interlinked due to the larger degree of association of anionic/cationic repeat units in the assembly.

Acknowledgment. The authors thank NSERC Canada for financial support in the form of grants and scholarships. Gratitude is extended to Ben Smith of the McGill Physics Department for instrumental and analytical help regarding AFM force measurements and Helen Campbell of Mining, Metals and Materials Engineering for help with SEM. Additional thanks are extended to Susan E. Burke and Kevin G. Yager for useful discussions regarding data interpretation.

References and Notes

- Decher, G.; Schmitt, J. *Prog. Colloid Polym. Sci.* **1992**, *89*, 160.
- Decher, G. *Science* **1997**, *277*, 1232.
- Rmaile, H. H.; Schlenoff, J. B. *J. Am. Chem. Soc.* **2003**, *125*, 6602.
- Qiu, X.; Leporatti, S.; Donath, E.; Möhwald, H. *Langmuir* **2001**, *17*, 5375.
- Hiller, J.; Mendelsohn, J. D.; Rubner, M. F. *Nature Mater.* **2002**, *1*, 59.
- Schuler, C.; Caruso, F. *Biomacromolecules* **2001**, *2*, 921.
- Antipov, A. A.; Sukhorukov, G. B.; Leporatti, S.; Radtchenko, I. L.; Donath, E.; Möhwald, H. *Colloids Surf., A* **2002**, *198*, 535.
- Levaesalmi, J.; McCarthy, T. J. *Macromolecules* **1997**, *30*, 1752.
- Mendelsohn, J. D.; Barrett, C. J.; Chan, V. V.; Pal, A. J.; Mayes, A. M.; Rubner, M. F. *Langmuir* **2000**, *16*, 5017.
- van de Steeg, H. G. M.; Cohen Stuart, M. A.; De Keizer, A.; Bijsterbosch, B. H. *Langmuir* **1992**, *8*, 2538.
- Dahlgren, M. A. G.; Waltermo, A.; Blomberg, E.; Claesson, P. M.; Sjöestroem, L.; Aakesson, T.; Joensson, B. *J. Phys. Chem.* **1993**, *97*, 11769.
- Sukhishvili, S.; Granick, S. *J. Chem. Phys.* **1998**, *109*, 6869.
- Losche, M.; Schmitt, J.; Decher, G.; Bouwman, W. G.; Kjaer, K. *Macromolecules* **1998**, *31*, 8893.
- Dubas, S. T.; Schlenoff, J. B. *Macromolecules* **1999**, *32*, 8153.
- Phuvanartnuruks, V.; McCarthy, T. J. *Macromolecules* **1998**, *31*, 1906.
- Yoo, D.; Shiratori, S. S.; Rubner, M. F. *Macromolecules* **1998**, *31*, 4309.
- Shiratori, S. S.; Rubner, M. F. *Macromolecules* **2000**, *33*, 4213.
- Lvov, Y.; Decher, G.; Haas, H.; Möhwald, H.; Kalachev, A. *Physica B* **1994**, *198*, 89.
- Kellogg, G. J.; Mayes, A. M.; Stockton, W. B.; Ferreira, M.; Rubner, M. F.; Satija, S. K. *Langmuir* **1996**, *12*, 5109.
- Loesche, M.; Schmitt, J.; Decher, G.; Bouwman, W. G.; Kjaer, K. *Macromolecules* **1998**, *31*, 8893.
- Lee, S. H.; Balasubramanian, S.; Kim, D. Y.; Viswanathan, N. K.; Bian, S.; Kumar, J.; Tripathy, S. K. *Macromolecules* **2000**, *33*, 6534.
- Koetse, M.; Laschewsky, A.; Jonas, A. M.; Verbiest, T. *Colloids Surf., A* **2002**, *198–200*, 275.
- Picart, C.; Ladam, G.; Senger, B.; Voegel, J. C.; Schaaf, P.; Cuisinier, F. J. G.; Gergely, C. *J. Chem. Phys.* **2001**, *115*, 1086.
- Baur, J. W.; Rubner, M. F.; Reynolds, J. R.; Kim, S. *Langmuir* **1999**, *15*, 6460.
- Lavalle, P.; Gergely, C.; Cuisinier, F. J. G.; Decher, G.; Schaaf, P.; Voegel, J. C.; Picart, C. *Macromolecules* **2002**, *35*, 4458.
- Schoeler, B.; Kumaraswamy, G.; Caruso, F. *Macromolecules* **2002**, *35*, 889.
- Yamada, T. Y.; Shiratori, S. *Mol. Cryst. Liq. Cryst. Sci. Technol., Sect. A* **2001**, *370*, 289.
- Lvov, Y.; Ariga, K.; Onda, M.; Ichinose, I.; Kunitake, T. *Colloids Surf., A* **1999**, *146*, 337.
- Kim, D. K.; Han, S. W.; Kim, C. H.; Hong, J. D.; Kim, K. *Thin Solid Films* **1999**, *350*, 153.
- Picart, C.; Lavalle, P.; Hubert, P.; Cuisinier, F. J. G.; Decher, G.; Schaaf, P.; Voegel, J. C. *Langmuir* **2001**, *17*, 7414.
- McAloney, R. A.; Sinyor, M.; Dudnik, V.; Goh, M. C. *Langmuir* **2001**, *17*, 6655.
- Notley, S. M.; Biggs, S.; Craig, V. S. *Macromolecules* **2003**, *36*, 2903.
- (a) Feiler, A.; Plunkett, M. A.; Rutland, M. W. *Langmuir* **2003**, *19*, 4173. (b) Plunkett, M. A.; Feiler, A.; Ruthland, M. W. *Langmuir* **2003**, *19*, 4180.
- Lukkari, J.; Salomäki, M.; Ääritalo, T.; Loikas, K.; Laiho, T.; Kankare, J. *Langmuir* **2002**, *18*, 8496.
- Lowack, K.; Helm, C. A. *Macromolecules* **1998**, *31*, 823.
- Ruths, M.; Sukhishvili, S. A.; Granick, S. *J. Phys. Chem. B* **2001**, *105*, 6202.
- Mermut, O.; Barrett, C. J. *J. Phys. Chem. B* **2003**, *107*, 2525.
- Domke, J.; Radmacher, M. *Langmuir* **1998**, *14*, 3320.
- Akhremitchev, B. B.; Walker, G. C. *Langmuir* **1999**, *15*, 5630.
- Lin, X. U.; Creuzet, F.; Arribart, H. *J. Phys. Chem.* **1993**, *97*, 7272.
- Fang, M.; Kim, C. H.; Saupe, G. B.; Kim, H. N.; Waraksa, C. C.; Miwa, T.; Fujishima, A.; Mallouk, T. E. *Chem. Mater.* **1999**, *11*, 1526.
- Höök, F.; Kasemo, B.; Nylander, T.; Fant, C.; Sott, K.; Elwing, H. *Anal. Chem.* **2001**, *73*, 5796.
- Dubas, S. T.; Schlenoff, J. B. *Macromolecules* **1999**, *32*, 8153.
- Treloar, L. R. G. *The Physics of Rubber Elasticity*, 2nd ed.; Oxford Clarendon Press: England, 1958; pp 187–196.
- Plunkett, M. A.; Claesson, P. M.; Ernstsson, M.; Rutland, M. W. *Langmuir* **2003**, *19*, 4673.
- van der Vegte, E. W.; Hadziioannou, G. *J. Phys. Chem. B* **1997**, *101*, 9563.